Berry-phase effects and electronic dynamics in a noncollinear antiferromagnetic texture

Olena Gomonay
National Technical University of Ukraine, Kyiv Polytechnic Institute, Ave Peremogy 37, 03056 Kyiv, Ukraine
(Received 23 February 2015; revised manuscript received 10 April 2015; published 27 April 2015)

Antiferromagnets (AFMs), in contrast to ferromagnets, show a nontrivial magnetic structure with zero net magnetization. However, they share a number of spintronic effects with ferromagnets, including spin pumping and spin-transfer torques. Both phenomena stem from the coupled dynamics of free carriers and localized magnetic moments. In the present paper I study the adiabatic dynamics of spin-polarized electrons in a metallic AFM exhibiting a noncollinear 120° magnetic structure. I show that the slowly varying AFM spin texture produces a non-Abelian gauge potential related to the time and space gradients of the Néel vectors. Corresponding emergent electric and magnetic fields induce rotation of spin and influence the orbital dynamics of free electrons. I discuss both the possibility of a topological spin Hall effect in the vicinity of topological AFM solitons with nonzero curvature and rotation of the electron spin traveling through the AFM domain wall.

DOI: 10.1103/PhysRevB.91.144421 PACS number(s): 75.50.Ee, 85.75.−d

I. INTRODUCTION

Metallic and semiconducting antiferromagnets (AFM) with high ordering (Néel) temperature are promising candidates for spintronic applications. Compared to their ferromagnetic counterparts, AFM-based devices show reduced critical currents for magnetization switching [1] and can effectively operate at higher frequencies [2]. According to theoretical predictions, AFMs can also show current-induced phenomena typical for ferromagnets, such as spin-transfer torques [3–5], spin pumping [6], and domain wall motion [7,8], but with much richer physics stemming from the nontrivial magnetic structure.

However, the mechanisms responsible for the coupled dynamics of free electrons and localized magnetic moments in AFMs are still not clear and thus recently became a matter of interest. For example, ferromagnets can work as spin polarizers due to exchange coupling between the localized spins (that contribute to macroscopic magnetization) and the spin of the conduction electron. In contrast, the AFMs have zero or vanishingly small magnetization. The symmetry properties of the Néel vector (AFM order parameter) differ from those of the spin vector and thus the polarization mechanism through *sd* exchange is excluded. On the other hand, AFMs have a nontrivial magnetic structure which removes degeneracy of otherwise equivalent directions and/or planes and thus can affect the spin dynamics of the free electron. The nontrivial spintronic effects in AFMs are usually attributed to the *sd* exchange and/or spin-orbit coupling. In homogeneous systems the spin-orbit interaction can induce polarization of the electric current which flows through the collinear AFM [9] or the anomalous Hall effect in noncollinear planar AFM [10,11]. Exchange interaction itself can induce the topological Hall effect in the structure with the nonzero chirality [12,13], e.g., in noncoplanar AFMs [14,15].

The *sd* exchange also plays an important role in the magnetic textures which can produce Abelian [16] and non-Abelian [17] gauge potentials for conduction electrons. Corresponding fields contribute to adiabatic spin-transfer torque and spin-pumping phenomena and thus could be experimentally detected. In particular, a *ferro*magnetic texture produces an effective spin-dependent $U(1)$ gauge field for conduction electrons. This gauge field gives rise to effective electrical and magnetic fields proportional to the macroscopic magnetization of the ferromagnet. An alternative point of view relates the emergent fields with the Berry phase accumulated by a free electron whose spin is aligned with the local macroscopic magnetization [18]. An analogous influence of the collinear *antiferro*magnetic texture on the dynamics of free carriers was recently predicted in Ref. [17] from semiclassical analysis of the Berry phase. The Berry phase also strongly affects the semiclassical motion of electrons in chiral magnets with spin-orbit interaction and can even induce formation of Skyrmions in these materials ("the driving force for formation"), as was recently demonstrated in Ref. [19].

The present paper focuses on the dynamics of spin-polarized electrons in the gauge potentials produced by the space-time varying magnetic moments of a noncollinear AFM. The main idea is to demonstrate that the adiabatic dynamics of free electrons is intimately related to the "dynamic" magnetization of AFM (no matter how complicated the AFM structure) and in this sense is similar to adiabatic dynamics of transport electrons in ferromagnets. Correspondingly, the curvature of a smooth distribution of AFM vectors generates effective electric and magnetic fields that affect, via *sd*-exchange coupling, the orbital motion of free electrons. I predict a possibility of topological spin Hall effect in noncollinear AFM textures that, in analogy with its ferromagnetic counterpart, originates from the *sd* exchange. This effect can be used to generate spin currents and probe the curvature of the AFM distribution. I demonstrate that an inhomogeneous AFM structure induces a rotation of the spin polarization (analog of Faraday effect). This effect can be an efficient tool for probing the AFM domain structure by electrical methods.

II. MODEL AND FORMALISM

As a prototype of a conductive antiferromagnet with noncollinear magnetic structure, I consider the antiperovskite Mn_3XN (X = Ag, Zn, Ni, Ga) with cubic space group $Pm3m$ (see Fig. 1) and with the magnetic moments localized at Mn atoms [20]. Although some authors [21–23] emphasize that strong hybridization around the Fermi level points to the

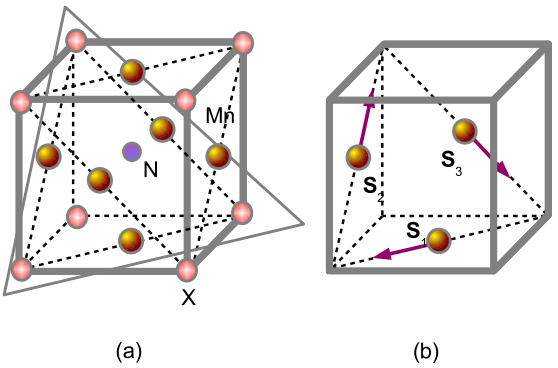

FIG. 1. (Color online) Unit cell (a) and Γ^{5g} magnetic structure (b) of antiperovskite Mn_3XN. Magnetic moments $\mathbf{S}_1$, $\mathbf{S}_2$, and $\mathbf{S}_3$ are localized at Mn atoms.

itinerant nature of antiferromagnetism in Mn-based antiperovskites, these substances could be effectively described by the Néel model of magnetic sublattices [24–26].

The Mn-based perovskites combine the nontrivial triangular magnetic structure with the peculiar transport properties. The linear temperature dependence of the resistivity and strong hybridization of Mn $3d$ and N $2p$ electrons around the Fermi level [22] suggests a metallic character of conductivity. However, the conductivity and temperature coefficient of resistivity are much smaller than those of a typical metal [27,28]. Hence, these compounds could be considered as bad metals with hopping character of conductivity. Resistivity measurements [28] also indicate a strong coupling between the magnetic structure and the transport properties. In addition, suppressed sd scattering in the magnetic phase [28] enables observation of the quantum phase effects. Thus Mn_3XN compounds are generic materials for analysis of the Berry-phase effects in noncollinear AFMs.

A. Magnetic structure formed by localized moments

The localized magnetic moments (sublattice magnetizations) represented by three classical vectors $\mathbf{S}_j$, $j = 1,2,3$ form a noncollinear coplanar structure classified,[1] depending on the material, as Γ^{5g} or Γ^{4g} [20]. Vectors $\mathbf{S}_j$ make a 120° angle with respect to each other. Thus the total magnetization cancels within the plane. The ordering plane is defined by the plane normal $\mathbf{n}$. Well below the Néel temperature, $|\mathbf{S}_j| = S$.

Within the macroscopic approach a noncollinear AFM structure can be conveniently described by two mutually orthogonal AFM, or Néel, vectors $\mathbf{L}_1 \perp \mathbf{L}_2$ ($|\mathbf{L}_1| = |\mathbf{L}_2| = \sqrt{3/2}S$) that could be considered as a multicomponent order parameter

$$\mathbf{L}_1 = \frac{1}{\sqrt{6}}(2\mathbf{S}_1 - \mathbf{S}_2 - \mathbf{S}_3), \quad \mathbf{L}_2 = \frac{1}{\sqrt{2}}(\mathbf{S}_2 - \mathbf{S}_3) \qquad (1)$$

[1]Strictly speaking, the Γ^{4g} structure realized in a certain temperature range is consistent with weak ferromagnetic structure in which the vectors $\mathbf{S}_j$ slightly deviate from the plane. We, however, neglect small uncompensated magnetization for the sake of simplicity.

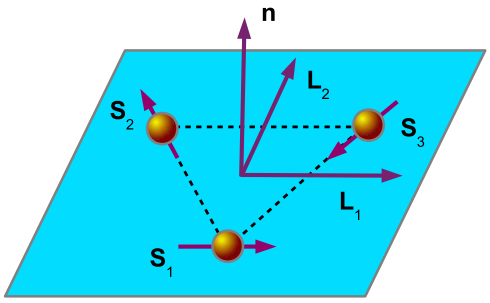

FIG. 2. (Color online) Local frame generated by AFM vectors $\mathbf{L}_1$, $\mathbf{L}_2$, and vector $\mathbf{n}$ normal to the plane of spin ordering.

and the macroscopic magnetization vector

$$\mathbf{M} = \frac{1}{\sqrt{3}}(\mathbf{S}_1 + \mathbf{S}_2 + \mathbf{S}_3). \qquad (2)$$

From the symmetry point of view vectors (1) and (2) belong to different irreducible representations of the permutation group P_3 (corresponding to the exchange symmetry of the crystal) [24].

In the AFM ground state the macroscopic magnetization $\mathbf{M} = 0$. Three orthogonal vectors $\mathbf{L}_1 \perp \mathbf{L}_2 \perp \mathbf{n}$ generate a natural local frame for free spin (see Fig. 2).

In equilibrium homogeneous state the corresponding vectors are $\mathbf{n}^{(0)} \| [111]$, $\mathbf{L}_1^{(0)} \| [0\bar{1}1]$, and $\mathbf{L}_2^{(0)} \| [2\bar{1}\bar{1}]$. In the texture (inhomogeneous state) the orientation of the sublattice magnetizations can smoothly vary at the length scale much greater than interatomic distances; thus all the magnetic vectors $\mathbf{S}_j$, $\mathbf{L}_1$, $\mathbf{L}_2(t,\mathbf{r})$ are continuous functions of time and space.

Strong exchange coupling locks the mutual orientation of localized moments, even in the presence of relatively small external fields. However, under the action of these fields the whole structure can smoothly rotate with respect to some initial configuration [labeled further with the subscript (0)]. In the adiabatic approximation which we consider below, the large-scale variation of localized moments is equivalent to solidlike rotation of vectors $\mathbf{S}_j$ (and, correspondingly, $\mathbf{L}_1,\mathbf{L}_2,\mathbf{n}$) and can be conveniently parametrized [29,30] with the Gibbs' vector $\boldsymbol{\varphi}$ (so-called Cayley-Gibbs-Rodrigues parametrization) as follows:

$$\mathbf{S}_j = \Re(\boldsymbol{\varphi})\mathbf{S}_j^{(0)} \equiv \frac{1-\boldsymbol{\varphi}^2}{1+\boldsymbol{\varphi}^2}\mathbf{S}_j^{(0)} + \frac{2}{1+\boldsymbol{\varphi}^2}\left[\boldsymbol{\varphi} \times \mathbf{S}_j^{(0)} + \boldsymbol{\varphi}\left(\boldsymbol{\varphi} \cdot \mathbf{S}_j^{(0)}\right)\right]. \qquad (3)$$

Here $\Re(\boldsymbol{\varphi})$ is the orthogonal rotation tensor, $\boldsymbol{\varphi}(t,\mathbf{r}) \equiv \tan(\theta/2)\,\mathbf{N}$, where $\mathbf{N}(t,\mathbf{r})$ is the instant rotation axis, $\theta(t,\mathbf{r})$ is the rotation angle, and we treat all the parameters as continuous functions of space and time.

Rotation of AFM moments plays an important role in the magnetic dynamics of localized spin. As it was pointed out by Andreev and Marchenko [29], a solidlike rotation of spins induces nonzero, "dynamic" magnetization of AFM, $\mathbf{M}_{\text{dyn}} \propto \hat{\chi}\boldsymbol{\Omega}_t$ ($\hat{\chi}$ is a tensor of magnetic susceptibility), which is proportional to the pseudovector $\boldsymbol{\Omega}_t$ of angular velocity,

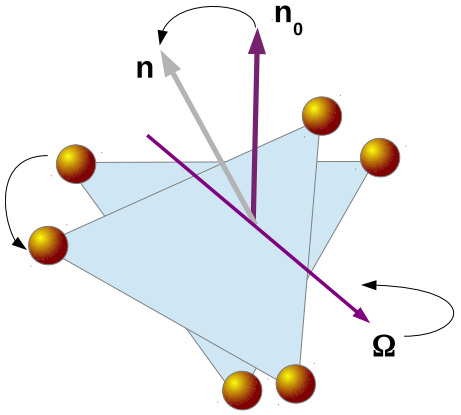

FIG. 3. (Color online) Solidlike rotation of the magnetic structure. Angular velocity $\mathbf{\Omega}$ may result either from the time or space rotation of the AFM structure, as described in the text.

frequently referred to as macroscopic spin (see Fig. 3):

$$\mathbf{\Omega}_t = 2\frac{\partial_t \boldsymbol{\varphi} + \boldsymbol{\varphi} \times \partial_t \boldsymbol{\varphi}}{1+\boldsymbol{\varphi}^2}, \quad \partial_t \Re(\boldsymbol{\varphi}) = \mathbf{\Omega}_t \times \Re(\boldsymbol{\varphi}). \tag{4}$$

However, a free electron moving with velocity $\dot{r}_l$ ($l = x,y,z$) in the slowly varying AFM texture should also "feel" the effective magnetization produced by space rotations of the AFM moments and described by the "space" angular velocity:

$$\mathbf{\Omega}_l = 2\frac{\partial_l \boldsymbol{\varphi} + \boldsymbol{\varphi} \times \partial_l \boldsymbol{\varphi}}{1+\boldsymbol{\varphi}^2}, \quad \partial_l \Re(\boldsymbol{\varphi}) = \mathbf{\Omega}_l \times \Re(\boldsymbol{\varphi}). \tag{5}$$

Thus in the continuous medium the dynamic magnetization of AFM seen by the conduction electron is proportional to the angular velocity $\mathbf{\Omega} = \mathbf{\Omega}_t + \mathbf{\Omega}_l \dot{r}_l$.

In what follows we consider the functions $\boldsymbol{\varphi}(t,\mathbf{r}), \mathbf{\Omega}(t,\mathbf{r})$ that describe the AFM texture as given, putting aside the problem of current-induced dynamics of localized spins.

B. Effective Hamiltonian and band structure

The transport properties of the system are described within the nearest-neighbor tight-bonding approximation validated by the low carrier density [27] and high resistivity [31] of Mn-based antiperovskites. In our toy model we consider only those electrons that hop between Mn sites, as they give the main contribution to the transport properties [21,22,28]. Then the local Hamiltonian for the conduction electrons takes a form

$$\hat{H}(\mathbf{r},t) = \sum_{j\tau} \varepsilon_0(\mathbf{k})\, \hat{a}^\dagger_{j\tau}\hat{a}_{j\tau} + \sum_{j,l,\tau} \gamma_{jl}(\mathbf{k})\, \hat{a}^\dagger_{j\tau}\hat{a}_{l\tau} - J_{sd} \sum_{j\tau,\tau'} \mathbf{S}_j(t,\mathbf{r})\, \hat{a}^\dagger_{j\tau}\hat{\boldsymbol{\sigma}}_{\tau\tau'}\hat{a}_{j\tau'}, \tag{6}$$

where the first term in the right-hand side (rhs) describes the kinetic energy related with the crystal translational symmetry. Fermi operators $\hat{a}_{j\tau}$ and $\hat{a}^\dagger_{j\tau}$ describe annihilation/creation of the electrons with the Bloch functions $|u_j\rangle$ ($\langle u_k \mid u_j\rangle = \delta_{kj}$) and in the spin states $|\tau\rangle$ ($\tau = \uparrow,\downarrow$): $\hat{a}^\dagger_{j\tau}|0\rangle = |u_j\rangle|\tau\rangle$ at different sublattices $j = 1,2,3$. In what follows we neglect the dispersion of $\varepsilon_0(\mathbf{k})$ and set its value to zero. Coefficient $\gamma_{jl}(\mathbf{k}) = -\sum_\delta t_\delta e^{i\mathbf{k}\boldsymbol{\delta}}$ is the hopping term between neighboring sites (connected with $\boldsymbol{\delta}$) that belongs to different sublattices

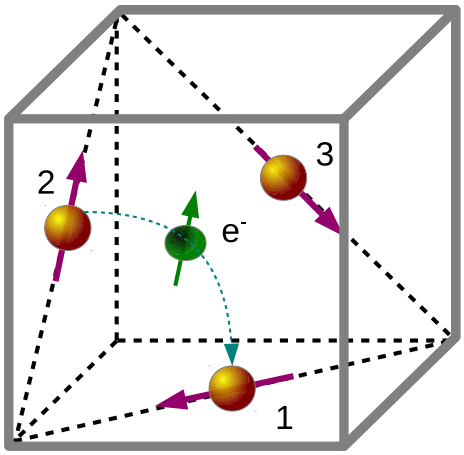

FIG. 4. (Color online) Electron (e^-) hopping between the magnetic sites. Different sites generate different quantization axes, due to 120° misalignment of local moments. Thus the hopping electron is always in a superposition of spin-up and spin-down states.

j and l (see Fig. 4). Constant J_{sd} describes the exchange coupling between localized and free electrons (so-called sd exchange), it can be either positive or negative, and without loss of generality we take $J_{sd} > 0$. $\hat{\boldsymbol{\sigma}}$ is the spin operator.

The local band structure obtained by diagonalization of Hamiltonian (6) consists of six bands which, neglecting the sd exchange, are pairwise (spin-up and spin-down) degenerate. The exchange interaction gives rise to an additional splitting and mixing of bands. As sublattice sites 1, 2, and 3 are equivalent, $\gamma_{12}(\mathbf{k}) = \gamma_{23}(\mathbf{k}) = \gamma_{31}(\mathbf{k}) = \gamma(\mathbf{k}) < 0$. In this case the band structure splits into four bands ($\varepsilon_1 < \varepsilon_2 < \varepsilon_3 < \varepsilon_4$):

$$\begin{aligned} \varepsilon_1(\mathbf{k}) &= 2\gamma - J_{sd}S, \quad \varepsilon_2(\mathbf{k}) = -\gamma - \sqrt{J_{sd}^2 S^2 + 9\gamma^2}, \\ \varepsilon_3(\mathbf{k}) &= 2\gamma + J_{sd}S, \quad \varepsilon_4(\mathbf{k}) = -\gamma + \sqrt{J_{sd}^2 S^2 + 9\gamma^2}. \end{aligned} \tag{7}$$

The states in the bands $\varepsilon_1,\varepsilon_3$ are nondegenerate, and those in bands $\varepsilon_2,\varepsilon_4$ are double degenerate. Corresponding eigenvectors (local spin quantization axis is parallel to $\mathbf{L}_1$) for the lower bands $\varepsilon_1,\varepsilon_2$ are the following:

$$\begin{aligned} |\Psi_1\rangle &= \frac{1}{\sqrt{3}}|\uparrow\rangle\left[|u_1\rangle + \frac{1}{2}(|u_2\rangle - |u_3\rangle)\right] + \frac{1}{2}|\downarrow\rangle(|u_2\rangle + |u_3\rangle), \\ |\Psi_{2a}\rangle &= |\eta_1\rangle|\uparrow\rangle + |\eta_2\rangle|\downarrow\rangle, \quad |\Psi_{2b}\rangle = |\eta_2\rangle|\uparrow\rangle + |\eta_3\rangle|\downarrow\rangle, \end{aligned} \tag{8}$$

where we have introduced the following (non-normalized) combinations of the mutually orthogonal Bloch functions (see Appendix A for details):

$$|\eta_1\rangle = \sqrt{\frac{2}{3}}\cos\psi\,|u_1\rangle - \frac{1}{2\sqrt{6}}(\cos\psi + 3\sin\psi)(|u_2\rangle - |u_3\rangle),$$

$$|\eta_2\rangle = \frac{1}{2}\sin\left(\psi - \frac{\pi}{4}\right)(|u_2\rangle + |u_3\rangle),$$

$$|\eta_3\rangle = \sqrt{\frac{2}{3}}\sin\psi\,|u_1\rangle - \frac{1}{2\sqrt{6}}(\sin\psi + 3\cos\psi)(|u_2\rangle - |u_3\rangle),$$

$$\langle\eta_1 \mid \eta_1\rangle = \langle\eta_3 \mid \eta_3\rangle = \frac{1}{4}(3 + \sin 2\psi),$$

$$\langle\eta_2 \mid \eta_2\rangle = \frac{1}{4}(1 - \sin 2\psi). \quad (9)$$

The effective parameter ψ depends on the relation between the sd exchange and the hopping integral as follows:

$$\sin 2\psi = \frac{3\gamma}{\sqrt{J_{sd}^2 S^2 + 9\gamma^2}}. \quad (10)$$

It is determined by the band structure and, as in the case of collinear AFM [17], plays a crucial role in the adiabatic electron dynamics. It describes an overlap of the functions (9),

$$\langle\eta_1 \mid \eta_3\rangle = \tfrac{1}{4}(1 + 3\sin 2\psi), \quad (11)$$

and hence the spin tunneling between different sites.

Expressions for the eigenfunctions $|\Psi_3\rangle$, $|\Psi_{4a,b}\rangle$ corresponding to the upper bands $\varepsilon_3,\varepsilon_4$ are analogous to those for $|\Psi_1\rangle,|\Psi_{2a,b}\rangle$ with substitution $\psi \to -\psi$, $\uparrow\leftrightarrow\downarrow$.

A rather complicated (compared to the case of collinear AFM) structure of the eigenfunctions $|\Psi_j\rangle$ is due to noncollinearity of neighboring localized moments. As a result, a free electron polarized along, say, the $\mathbf{S}_1$ direction is, after hopping, always in a superposition of spin states with respect to the new host's quantization axis (see Fig. 4). It is instructive to analyze the energy spectrum with account of average spin $\mathbf{s} \equiv \langle\hat{\boldsymbol{\sigma}}\rangle$ of the corresponding eigenstate (hereafter we use the convention $\hbar = 1$). As it was already mentioned, in the AFM ground state the magnetization of localized spins $\mathbf{M} = 0$ and one can anticipate that the ground state of conduction electrons is a spinless. It can be easily checked from (8) that the lowest energy band (ε_1) corresponds to the zero-spin "singlet" state $|\Psi_1\rangle$. The next band in energy scale ε_2 is formed by degenerate states $|\Psi_{2a}\rangle$ and $|\Psi_{2b}\rangle$, which are spin polarized in z direction parallel to the AFM vector $\mathbf{L}_1$ with opposite spin values $S_z = \pm(1 + \sin 2\psi)/2$. In equilibrium ($\mathbf{M} = 0$) both states should be equally populated. The other states that form the upper bands ε_3 and ε_4 have analogous properties: $|\Psi_3\rangle$ is spinless, and $|\Psi_{4a}\rangle$, $|\Psi_{4b}\rangle$ are spin polarized.

Obviously, in the case of spin injection only the degenerate states $|\Psi_{2a}\rangle$, $|\Psi_{2b}\rangle$ and $|\Psi_{4a}\rangle$, $|\Psi_{4b}\rangle$ could be populated and thus can participate in spin transport. Moreover, in the system under consideration the Berry connection of nondegenerate states is proportional to the average spin (see Appendix B) and thus vanishes for $|\Psi_1\rangle$ and $|\Psi_3\rangle$. If, in addition, $s - d$ exchange coupling is rather strong ($J_{sd} \gg \gamma$), the lower bands $\varepsilon_1,\varepsilon_2$ are well separated from the upper ones $\varepsilon_3,\varepsilon_4$, and the transport of spin-polarized electrons is restricted mainly to the second ε_2 band.

In what follows we assume that the Fermi level is situated in the vicinity of the degenerate band ε_2, and in the next section we consider the adiabatic spin dynamics related with tunneling between states $|\Psi_{2a}\rangle$ and $|\Psi_{2b}\rangle$ in the AFM texture.

C. Pseudospin and dynamic equations

We follow the semiclassical approach [17,32–34] to describe the effective electron dynamics in the degenerate band ε_2. An individual electron is seen as a wave packet,

$$|W\rangle = \int d\mathbf{k}\, p(\mathbf{k} - \mathbf{k}_c)\,[c_a\,|\Psi_{2a}\rangle + c_b\,|\Psi_{2b}\rangle], \quad (12)$$

where $\int d\mathbf{k}\,|p(\mathbf{k} - \mathbf{k}_c)|^2 = \mathbf{k}_c$ is the center of mass momentum, and $\langle W|\,\mathbf{r}\,|W\rangle = \mathbf{r}_c$ is the center of mass position, $|c_a|^2 + |c_b|^2 = 1$. We assume that the wave packet (12) spread is small compared to the length scale of AFM inhomogeneity.

Coherent dynamics between the two subbands introduces an internal degree of freedom which we describe by the spinor $(c_a c_b)$ or, equivalently, by the isospin vector

$$\mathbf{C} = \{2\mathrm{Re}(c_a c_b^*), -2\mathrm{Im}(c_a c_b^*), |c_a|^2 - |c_b|^2\}. \quad (13)$$

It is worth mentioning that both the spinor and the normalized isospin vector $\mathbf{C}$ represent the SU(2) group in two-dimensional Hilbert space formed by the state vectors $|\Psi_{2a}\rangle$ and $|\Psi_{2b}\rangle$.

The space-time dependence of the state vectors $|\Psi_{2a}\rangle$ and $|\Psi_{2b}\rangle$ stems exclusively from the rotation of the local spin quantization axis induced by variation of the AFM moments $[\mathbf{S}_j(t,\mathbf{r}_c)$ or, equivalently, $\mathbf{L}_1(t,\mathbf{r}_c),\mathbf{L}_2(t,\mathbf{r}_c),\mathbf{n}(t,\mathbf{r}_c)]$. It should be noted that the space dependence of Bloch functions $|u_j\rangle$ is substantial only at the length scale of interatomic distances and thus is unimportant at the large-scale variations of the AFM order parameters. Since, in addition, we neglect spin-orbit interactions, rotation of the magnetic moments is decoupled from variation of the crystallographic axes and, correspondingly, spin- and space-dependent states of the carriers are disentangled.

As the local orientation of the AFM moments is unambiguously defined by the rotation matrix $\Re(\boldsymbol{\varphi})$ [see Eq. (3)], the state vector $|\Psi_{2a,b}(r_\mu)\rangle$ at a given point $r_\mu = (t,\mathbf{r}_c)$ can be defined by an SU(2) gauge unitary transformation corresponding to $O(3)$ rotation:

$$\hat{U} = \cos\frac{\theta}{2}\hat{1} - i\sin\frac{\theta}{2}\mathbf{N}\hat{\boldsymbol{\sigma}} = \frac{1}{\sqrt{1+\boldsymbol{\varphi}^2}}(\hat{1} - i\boldsymbol{\varphi}\hat{\boldsymbol{\sigma}}). \quad (14)$$

Thus

$$|\Psi_2(r_\mu)\rangle = \hat{U}\,|\Psi_2(r_\mu^0)\rangle, \quad (15)$$

where the reference state vectors $|\Psi_2(r_\mu^0)\rangle$ and reference AFM vectors $\mathbf{L}_1^{(0)},\mathbf{L}_2^{(0)}$ are taken in the same fixed point r_μ^0. The gauge is fixed by the choice of spin eigenstates at this point.[2] The vectors $|\Psi_{2a}\rangle$ and $|\Psi_{2b}\rangle$ also depend indirectly on quasi wave vector $k_\mu = (0,\mathbf{k}_c)$ through the coefficient $\psi\,[\gamma(\mathbf{k}_c)]$.

[2]The gauge fields in non-Abelian theory are gauge covariant, not gauge invariant. However, as it was explained in detail in Ref. [17], the ultimate quasiclassical equations (17) and (18) include only the isospin scalars $\mathbf{CR}_{\mu\nu}$, which respect the gauge invariance. Thus, for the sake of definiteness we can fix the gauge in a similar way as in Ref. [17] without loss of generality.

According to the general theory [33], the set of equations of motion for the dynamic variables $\mathbf{r}_c$, $\mathbf{k}_c$, and $\mathbf{C}$ can be written as follows (see Ref. [17] for the detailed derivation):

$$\dot{\mathbf{C}} = 2\mathbf{C}\times\left(\mathbf{A}^r_\mu \dot{r}_\mu + \mathbf{A}^k_\mu \dot{k}_\mu\right), \tag{16}$$

$$\dot{k}_\mu = -\partial^r_\mu \varepsilon_2 + \mathbf{C}\left(\mathbf{R}^{rr}_{\mu\nu}\dot{r}_\nu + \mathbf{R}^{rk}_{\mu\nu}\dot{k}_\nu\right), \tag{17}$$

$$\dot{r}_\mu = \partial^k_\mu \varepsilon_2 - \mathbf{C}\left(\mathbf{R}^{kr}_{\mu\nu}\dot{r}_\nu + \mathbf{R}^{kk}_{\mu\nu}\dot{k}_\nu\right), \tag{18}$$

where the gauge potentials $\{\mathbf{A}^r_\mu, \mathbf{A}^k_\mu\}$, Berry connection $\hat{\mathcal{A}}^\alpha_\mu \equiv \mathbf{A}^\alpha_\mu \hat{\boldsymbol{\sigma}}$, and Berry curvatures $\mathbf{R}^{\alpha\beta}_{\mu\nu}$ $(\alpha,\beta = r,k)$ are introduced in a standard way as

$$\hat{\mathcal{A}}^\alpha_\mu = i\begin{pmatrix} \langle\Psi_{2a}|\partial^\alpha_\mu\Psi_{2a}\rangle & \langle\Psi_{2a}|\partial^\alpha_\mu\Psi_{2b}\rangle \\ \langle\Psi_{2b}|\partial^\alpha_\mu\Psi_{2a}\rangle & \langle\Psi_{2b}|\partial^\alpha_\mu\Psi_{2b}\rangle \end{pmatrix}, \tag{19}$$

$$\mathbf{R}^{\alpha\beta}_{\mu\nu} = \partial^\alpha_\mu \mathbf{A}^\beta_\nu - \partial^\beta_\nu \mathbf{A}^\alpha_\mu + 2\mathbf{A}^\alpha_\mu \times \mathbf{A}^\beta_\nu. \tag{20}$$

Starting from Eq. (16), we drop the subscript c on $\mathbf{r}_c$ and $\mathbf{k}_c$.

III. ADIABATIC DYNAMICS

A. Berry curvature and topology of AFM texture

Before considering the possible dynamics of free electrons it is instructive to analyze the explicit expressions for the Berry connection and the Berry curvature in AFM texture. Calculations based on definitions (19) and (20) (see Appendix B) show that the gauge potential

$$\mathbf{A}^r_\mu = \tfrac{1}{4}\Re^{-1}(\boldsymbol{\varphi})[(1+\sin 2\psi)\boldsymbol{\Omega}_\mu - (1-\sin 2\psi)\mathbf{n}(\boldsymbol{\Omega}_\mu\mathbf{n})], \tag{21}$$

and $\mathbf{A}^k_\mu = 0$ in the absence of spin-orbit interactions [17]. Correspondingly, nontrivial components of the Berry curvature are the following:

$$\begin{aligned}\mathbf{R}^{rr}_{\mu\nu} &= \tfrac{1}{8}(1-\sin 2\psi)\,\Re^{-1}(\boldsymbol{\varphi})\,[2(1+\sin 2\psi)\,\boldsymbol{\Omega}_\nu \times \boldsymbol{\Omega}_\mu \\ &\quad - (3+\sin 2\psi)\,\mathbf{n}\left(\mathbf{n}\cdot\Omega_\nu \times \boldsymbol{\Omega}_\mu\right)], \\ \mathbf{R}^{rk}_{\mu\nu} &= -\mathbf{R}^{kr}_{\nu\mu} = \tfrac{1}{4}\partial^k_\nu \sin 2\psi \Re^{-1}(\boldsymbol{\varphi})\,[\boldsymbol{\Omega}_\mu + \mathbf{n}\left(\boldsymbol{\Omega}_\mu\mathbf{n}\right)].\end{aligned} \tag{22}$$

The multiplier $\Re^{-1}(\boldsymbol{\varphi})$ (inverse rotation matrix) in Eqs. (21) and (22) results from the gauge covariance of the non-Abelian gauge fields. As we will see later, the same rotation relates the isospin to the real spin.

Analysis of the relations (21) and (22) shows that the gauge potentials produced by the AFM texture depend on the orientation of AFM vectors through the rotation vector $\boldsymbol{\Omega}_\mu$ which, in turn, is related to the dynamic magnetization $\mathbf{M}_{\rm dyn}$. The Berry curvature $\mathbf{R}^{rr}_{\mu\nu}$ for *free electrons* is proportional to the curvature $\mathbf{K}_{\mu\nu} \equiv \boldsymbol{\Omega}_\mu \times \boldsymbol{\Omega}_\nu = \partial^r_\mu \boldsymbol{\Omega}_\nu - \partial^r_\nu \boldsymbol{\Omega}_\mu$ of the *AFM texture*.[3] In other words, the Berry curvature is intimately related with topological properties of the space distribution of the localized moments. To give a sample distribution with the nontrivial curvature, we note that in elasticity theory $K_{\mu\nu} \neq 0$

[3]Note that we discuss only the rotations in spin state; the lattice itself is supposed to be unchanged. However, the theory can be generalized to include space rotations of the lattice, as it will be discussed below. See also Ref. [32] for a description of the gauge fields in deformed crystals.

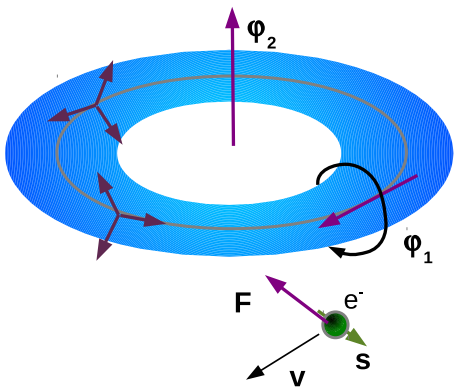

FIG. 5. (Color online) Orbital dynamics of an electron in the AFM texture with nonzero curvature. The blue (shadowed) torus shows the area with twisted (vector $\boldsymbol{\varphi}_1$) and bended (vector $\boldsymbol{\varphi}_2$) AFM vectors (three bounded arrows). Free spin-polarized (spin $\mathbf{s}$) electron moving in this area with the group velocity $\mathbf{v}$ feels the effective force $\mathbf{F}$ (see text for details).

is called the bend-twist tensor. So, one can imagine that in some toroidal area (see Figs. 5 and 8) the orientation of AFM vectors is obtained by two rotations—one around the in-plane axis tangent to the torus (twist with the rotation vector $\boldsymbol{\varphi}_1$) and another around the vertical torus axis z (bend with the rotation vector $\boldsymbol{\varphi}_2$). The curvature vector $\mathbf{K}_{xy} = \boldsymbol{\Omega}_x \times \boldsymbol{\Omega}_y$ in each point of the structure is directed along the radius. This structure, through *sd* exchange, forms a potential with a Berry curvature $\mathbf{R}^{rr}_{xy} \propto \mathbf{K}_{xy}$ and produces a "Lorentz-like" effective force for free spin-polarized electrons, as will be explained below.

It is instructive to compare expression (21) describing a gauge potential in AFM with the analogous expression [35] for a ferromagnetic (FM) material with the magnetization vector $\mathbf{m}$:

$$\mathbf{A}^{\rm FM}_\mu = -\mathbf{m}\times\partial^r_\mu\mathbf{m} = -(1-\mathbf{m}\otimes\mathbf{m})\,\boldsymbol{\Omega}_\mu. \tag{23}$$

Although in ferromagnets the gauge transformation is applied to the real spin (not to isospin), and the gauge potential is Abelian, comparison of expressions (23) and (21) shows that up to the details related with peculiarities of electron hopping, geometric effects in FM and AFM are related with the "dynamic" magnetization proportional to the angular velocity $\boldsymbol{\Omega}_\mu$.

It is also worth noting the relation between the curvature $\mathbf{K}_{\mu\nu}$ and the topological properties of localized nonlinear magnetic structures: Skyrmions, solitons, vortices. For example, the topological charge of a two-dimensional (in the real space) Skyrmion, that counts how many times the vector order parameter $\mathbf{m}(t,\mathbf{r})$ wraps around the unit sphere, is defined as [36]

$$Q = \frac{1}{8\pi}\int \mathbf{m}\cdot(\partial_\mu\mathbf{m}\times\partial_\nu\mathbf{m} - \partial_\nu\mathbf{m}\times\partial_\mu\mathbf{m})dx_\mu dx_\nu. \tag{24}$$

With the use of relations (3)–(5) it can be easily shown that Q is proportional to the projection of the curvature vector $\mathbf{K}_{\mu\nu}$ onto the order parameter $\mathbf{m}$ averaged over space:

$$Q = \frac{1}{4\pi}\int(\mathbf{m}\cdot\boldsymbol{\Omega}_\mu\times\boldsymbol{\Omega}_\nu)dx_\mu dx_\nu. \tag{25}$$

The relation (25) is applicable to any magnetic system with the vector order parameter: a ferromagnet, with **m** playing the role of magnetization vector, a collinear AFM, where **m** corresponds to the Néel vector.

Topological charges of the three-dimensional structures with the vector order parameter are characterized with the Hopf's invariant [37,38], which describes the S^3 to S^2 map:

$$H = \frac{1}{16\pi^2}\int dx^3 \varepsilon_{\mu\nu\gamma}\varepsilon_{jklm} n_j \frac{\partial n_k}{\partial x_\mu}\frac{\partial n_l}{\partial x_\nu}\frac{\partial n_m}{\partial x_\gamma}, \qquad (26)$$

where the four-component vector $(\boldsymbol{\nu}, \nu_4)$ is related with the Gibb's vector $\boldsymbol{\varphi} = \boldsymbol{\nu}/\nu_4$, $\nu_4 = \cos\theta/2$, and $\varepsilon_{\mu\nu\gamma}$ and ε_{jklm} are fully antisymmetric tensors.

For the case of noncollinear AFMs an appropriate topological invariant is given by the expressions [39]

$$Q = -\frac{1}{24\pi^2}\int dx^3 \varepsilon_{\mu\nu\gamma} \times \mathrm{Tr}\left[\Re^{-1}(\boldsymbol{\varphi})\frac{\partial}{\partial x_\mu}\Re(\boldsymbol{\varphi})\Re^{-1}\frac{\partial}{\partial x_\nu}\Re(\boldsymbol{\varphi})\Re^{-1}\frac{\partial}{\partial x_\gamma}\Re(\boldsymbol{\varphi})\right], \qquad (27)$$

which corresponds to an S^3 to S^3 map. The three-dimensional AFM order parameter (formed by mutually orthogonal $\mathbf{L}_1$ and $\mathbf{L}_2$ vectors) is parametrized with the rotational tensor $\Re(\boldsymbol{\varphi})$. With the use of expression (4) the topological invariant (27) can be expressed in terms of the rotation vectors $\boldsymbol{\Omega}_\mu$ as follows:

$$Q = -\frac{1}{24\pi^2}\int dx^3 \varepsilon_{\mu\nu\gamma}(\boldsymbol{\Omega}_\mu \cdot \boldsymbol{\Omega}_\nu \times \boldsymbol{\Omega}_\gamma). \qquad (28)$$

It can be easily seen that, in analogy with ferromagnets, the topological charge (28) is proportional to the projection of the curvature vector $\mathbf{K}_{\nu\gamma}$ onto the direction of dynamics magnetization $\boldsymbol{\Omega}_\mu$ seen by the free electron moving in the x_μ direction.

Note that the model "twist-bend" structure shown in Figs. 5 and 8 can, in principle, have nonzero topological charge if the the AFM ordering outside the toroidal area is homogeneous. In this case the structure is characterized with three nontrivial noncollinear rotational vectors: $\boldsymbol{\Omega}_1$ and $\boldsymbol{\Omega}_2$ for twisting and bending, and $\boldsymbol{\Omega}_3$, which describes smooth rotation of AFM vectors in the intermediate area between the torus and infinity.

B. Free spin dynamics and gauge potential

Let us consider a typical spintronic problem in which a nonequilibrium spin-polarized carrier is injected into an AFM. The question is, "Does the AFM medium affect the state of an electron? If it does, how could this effect be observed?"

To begin with, we find the relation between the isospin vector **C** (which itself is not gauge invariant and depends upon the choice of the eigenfunctions $|\Psi_{2a}\rangle$, $|\Psi_{2b}\rangle$) and the observable (and fully gauge invariant) spin $\mathbf{s} \equiv \langle W|\,\hat{\boldsymbol{\sigma}}\,|W\rangle$. Direct calculations based on the states (8) and (15) give rise to the following expression for the spin vector:

$$\mathbf{s}(t,\mathbf{r}) = \tfrac{1}{2}(1+\sin 2\psi)\,[\Re(\boldsymbol{\varphi})\,\mathbf{C}] - \tfrac{1}{2}(1-\sin 2\psi)\,[\Re(\boldsymbol{\varphi})\,\mathbf{C}\cdot\mathbf{n}]\,\mathbf{n}. \qquad (29)$$

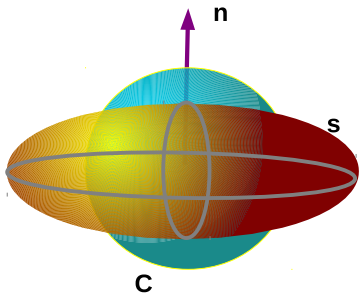

FIG. 6. (Color online) Isospin **C** (sphere) and real spin **s** (spheroid) in the local frame.

Using normalization of the isospin, $|\mathbf{C}|^2 = 1$, we arrive at a relation between the spin of the free carrier and the orientation of the plane formed by the localized spins and represented by the vector $\mathbf{n}(t,\mathbf{r})$ (see Fig. 6):

$$\frac{(\mathbf{ns})^2}{\sin^2 2\psi} + \frac{4\,(\mathbf{n}\times\mathbf{s})^2}{(1+\sin 2\psi)^2} = 1. \qquad (30)$$

Analysis of expression (30) shows that, like in the case of a collinear AFM [17] [see also Eq. (38)], spin polarization of the conduction electron depends upon the orientation of the AFM vectors. In a noncollinear AFM the vector **s** varies on an oblate spheroid (on a prolate in the collinear AFM), the short axis of which coincides with the plane normal. Like in the collinear case $\mathbf{s}^2 \leqslant 1$, which means that an electron is in a mixed spin state due to entanglement between the space and spin degrees of freedom.

The equation for spin dynamics obtained from Eq. (29) with account of Eqs. (16) and (21) (see Appendix B for hints of the derivation) is similar to Euler's equation for rotation of a rigid body:

$$\dot{\mathbf{s}} - \boldsymbol{\Omega}\times\mathbf{s} = -\sin 2\psi\,\boldsymbol{\Omega}\times\hat{g}\mathbf{s}, \qquad (31)$$

where we introduced the tensor

$$\hat{g} = \hat{1} + \left[\left(\frac{1+\sin 2\psi}{2\sin 2\psi}\right)^2 - 1\right]\mathbf{n}\otimes\mathbf{n}, \qquad (32)$$

and, as it was already noted, $\boldsymbol{\Omega} = \boldsymbol{\Omega}_t + \boldsymbol{\Omega}_l \dot{r}_l$. The second term on the left-hand side of Eq. (31) originates from the rotation of the local frame associated with vectors $\mathbf{L}_1$, $\mathbf{L}_2$, **n** (for the constant isospin **C**). In analogy with Ref. [32], it could be called a "tracking" term because it reflects the tendency of the AFM lattice to drag the electron spin along with the time and space AFM motion.

The rhs describes the spin evolution in the local frame due to accumulation of a SU(2) non-Abelian Berry phase, namely, the spin vector rotates around the angular velocity $\boldsymbol{\Omega}$, being simultaneously bound to the spheroid (30). Thus Eq. (31) is the Bloch equation for spin precession in the effective magnetic field $\mathbf{H}^{\mathrm{eff}} = -\sin 2\psi\,\hat{g}\boldsymbol{\Omega}$. As $\boldsymbol{\Omega}$ is proportional to the dynamic magnetization $\mathbf{M}_{\mathrm{dyn}}$ of the AFM layer, the origin of the effective magnetic field $\mathbf{H}^{\mathrm{eff}}$ acting on free spins has the same nature as in ferromagnets [40].

It should be stressed that spin dynamics substantially depends upon the strength of *sd*-exchange coupling. In the limit $J_{sd} \to 0$ (which means that $\sin 2\psi \to 1$), the electron spin coincides with the pseudospin **C** up to rotation $\Re(\boldsymbol{\varphi})$ and

$\dot{\mathbf{s}} = 0$. In the opposite case of extremely strong $J_{sd} \to \infty$ (or, equivalently, $\sin 2\psi \to 0$), the rhs term in Eq. (31) vanishes. So, in the case of strong coupling between free and localized spins, the free spin simply tracks orientation of the local frame in each point.

Orbital dynamics of the wave packet (12) is described by semiclassical equations obtained from Eqs. (17) and (18), with account of Eq. (31) as follows:

$$\dot{r}_\mu = \partial^k_\mu \varepsilon_2 + \frac{1}{2}\partial^k_\mu \ln(1+\sin 2\psi) \times \left[\mathbf{s}\cdot\mathbf{\Omega} + \frac{1}{\sin 2\psi}(\mathbf{n}\cdot\mathbf{s})(\mathbf{n}\cdot\Omega)\right], \quad (33)$$

$$\dot{k}_\mu = -\partial^r_\mu \varepsilon_2 - \frac{1}{2}\dot{\mathbf{s}}\cdot\mathbf{\Omega}_\mu. \quad (34)$$

The spin-dependent addition to the group velocity in Eq. (33) is proportional to $\partial^k_\mu \varepsilon_2$, because $\partial^k_\mu \sin 2\psi \sim \partial^k_\mu \gamma \sim \partial^k_\mu \varepsilon_2$. So, coupling between the free and the localized spins in the rotated AFM texture results in "renormalization" of the effective electron mass. An analogous term, omitted in Eq. (34) for the sake of simplicity, appears also in the equation for acceleration [see Appendix B, Eq. (B7)].

The nontrivial, spin-dependent term on the rhs of Eq. (34) is intimately related to the spin dynamics. It can also be represented in the form of a fictitious Lorentz force with the effective electriclike E_μ and magneticlike B_ξ components:

$$\dot{k}_\mu = -\partial^r_\mu \varepsilon_2 + q(E_\mu + \varepsilon_{\mu\nu\xi}\dot{r}_\nu B_\xi), \quad (35)$$

$$q E_\mu = \tfrac{1}{2}[\mathbf{s}\cdot\mathbf{\Omega}_t \times \mathbf{\Omega}_\mu + \sin 2\psi\, \hat{g}\mathbf{s}\cdot\mathbf{\Omega}_t \times \mathbf{\Omega}_\mu], \quad (36)$$

$$q B_\xi = \tfrac{1}{2}\varepsilon_{\xi\mu\nu}[\mathbf{s}\cdot\mathbf{\Omega}_\nu \times \mathbf{\Omega}_\mu + \sin 2\psi\, \hat{g}\mathbf{s}\cdot\mathbf{\Omega}_\nu \times \mathbf{\Omega}_\mu], \quad (37)$$

where, as above, $\varepsilon_{\xi\mu\nu}$ is the antisymmetric Levi-Civita tensor. The corresponding effective "charge" q (field "source") is proportional to the spin.[4]

Equations (35)–(37) are similar to equations that describe an orbital motion of individual electrons in a collinear AFM [17]. In both cases the gauge charge q depends upon the spin which, according to Eq. (31), shows its own dynamics and thus can vary in time. In both cases the gauge charge depends upon the sd-exchange constant (in our case, through the multiplier $\sin 2\psi$) and vanishes when $J_{sd} \to 0$.

The feature demonstrated in this paper is a certain universality of spin-dependent orbital dynamics in AFMs. Really, the dynamic equations of a collinear AFM (Eq. (8) of Ref. [17]) have practically the same form as Eqs. (31), (33), and (34) of the present paper when written in terms of angular velocity $\dot{\mathbf{L}} = \Omega \times \mathbf{L}$:

$$\dot{\mathbf{s}} - \mathbf{\Omega}\times\mathbf{s} = -\mathbf{\Omega}\times\hat{g}\mathbf{s}, \quad \hat{g} = \hat{1} + (\xi^2 - 1)\mathbf{L}\otimes\mathbf{L}, \quad (38)$$

$$\dot{r}_\mu = -\partial^k_\mu \varepsilon_2 + \tfrac{1}{2}\partial^k_\mu \ln\xi\,[\mathbf{s}\cdot\mathbf{\Omega} - (\mathbf{L}\cdot\mathbf{s})(\mathbf{L}\cdot\Omega)], \quad (39)$$

$$\dot{k}_\mu = -\tfrac{1}{2}\mathbf{\Omega}_\mu\cdot\dot{\mathbf{s}}, \quad (40)$$

where ξ, in the original notations, is the overlap of the wave functions analogous to $\sin 2\psi$ of the present paper [see Eq. (10)], and the notation $\mathbf{L}$ is used for the Néel vector of collinear AFM.

Thus, in AFMs with strong exchange coupling between the magnetic sublattices the emergent Lorentz force (35) is defined mainly by the *angular velocity* $\mathbf{\Omega}_t$ (and hence the dynamic magnetization) and the *AFM curvature* $\mathbf{\Omega}_\nu \times \mathbf{\Omega}_\mu$, and has similar form for the different AFM structures. However, dependence on peculiarities of the ground state (number of sublattices and their mutual orientation, type of magnetic anisotropy etc) is included in a cumbersome presentation of the gauge charge, tensor $\hat{g}$, and spin ellipsoid. In particular, in a collinear AFM the anisotropy of these parameters is dictated by the easy-axis parallel to a single AFM vector, in the present case, by the easy plane formed by two orthogonal Néel vectors.

The effective electric field (36) plays a role of a spin-dependent motive force (similar to that in FM, see Ref. [18]). So, an oscillating ($\mathbf{\Omega}_t \neq 0$) inhomogeneous ($\mathbf{\Omega}_\mu \neq 0$) AFM structure can produce an electric current (or voltage) and thus can be observed by standard electric measurements.

The effective magnetic field (37) is proportional to the projection of curvature $\mathbf{\Omega}_\nu \times \mathbf{\Omega}_\mu$ of the AFM texture on the free spin $\mathbf{s}$. Direction of the latter correlates (and in the limit of strong sd-exchange coupling, coincides) with the direction of $\mathbf{\Omega}$ and dynamic magnetization of the AFM. Thus the flux of the emergent magnetic field is related with the topological charge of the AFM distribution [see Eq. (28), where the curvature is projected in the direction of dynamic magnetization seen by the free electron). An analogous situation takes place in Skyrmions where the flux of emergent magnetic field is associated with Skyrmion number (i.e., topological charge) [36]. However, gauge effects in Skyrmions and AFMs are principally different. Namely, a Skyrmion can be treated as a ferromagnet with a complicated distribution of localized moments, and in adiabatic limit the spin of a conduction electron always tracks the local orientation of magnetization. The gauge potential is Abelian, and the topological charge of a Skyrmion is related with chirality [15]. In contrast, the AFM which we consider here has zero total static magnetization; a complicated slowly varying magnetic texture is locally formed by a proper number of AFM vectors attributed to same point; a conduction electron feels the local frame induced by magnetic moments but not the direction of magnetization itself. The nontrivial effect of geometric phase in the absence of total magnetization is due to the *degeneracy of states* and resulting *non-Abelian* character of the gauge potential.

The emergent magnetic field in adiabatic motion is usually associated with the topological Hall effect. On the other hand, most AFM structures are usually invariant with respect to time-reversal symmetry and this forces Hall conductivities to vanish. Recently, it was demonstrated that noncollinear [10] and frustrated [41] AFMs can show an anomalous Hall effect that arises due to spin-orbit coupling. The origin of nonzero Hall conductivity in these materials is the *Berry curvature* in *momentum* space. In contrast, Eq. (35) (and the analogous equation for collinear AFM from Ref. [17]) shows that the Hall effect can in principle be observed in compensated AFMs with negligible spin-orbit coupling. In this case the Hall conductivity originates from the *Berry curvature*

[4]Strictly speaking, an effective charge should be introduced as a vector quantity, so, for the sake of simplicity we introduce a combination of charge and fields. However, Faraday's relation for fields $\varepsilon_{\xi\mu\nu}\partial_\mu E_\nu + \partial_t B_\xi = 0$ is satisfied.

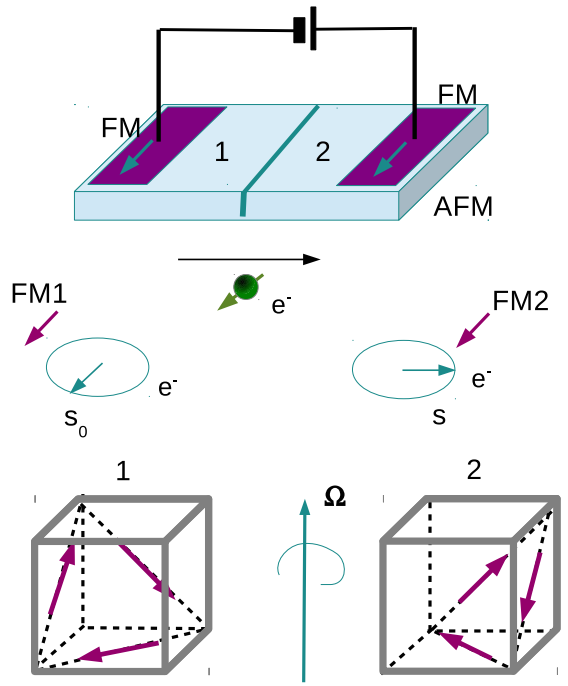

FIG. 7. (Color online) Probing the domain wall with the spin-polarized current. Two ferromagnetic electrodes, FM1 and FM2, placed over the AFM film produce spin-polarized current in the in-plane geometry (upper panel). Two AFM domains 1 and 2 (lower panel) are related through the 90° rotation. The spin of the electron e^- traveling through the domain wall tracks the local AFM structure and rotates (central panel). Misorientation between the free spin and the FM2 magnetization contributes to magnetoresistance and can be detected.

in *real* space and, what is also important, is related with the *curvature of the AFM texture*. The required breaking of time-reversal symmetry results from the inhomogeneity[5] and related dynamic magnetization $\mathbf{M}_{\rm dyn} \sim \mathbf{\Omega}$ of AFM structure as was explained above. Following Ref. [12], this Hall effect should be called topological.

Equations (31), (33), and (34) state the main results of this paper. They describe electron dynamics in a noncollinear AFM in terms of three observables $(\mathbf{s},\mathbf{r},\mathbf{k})$. However, so far our treatment was quite general and abstract. To make physical meaning of the obtained results clearer, in the next section I consider some special cases accessible for the experimental implementation.

IV. EXAMPLES

A. Traveling between AFM domains

Let us start from the "canonical" example of an AFM texture—a flat, one-dimensional domain wall separating two domains with different orientations of spin-ordering plane (see Fig. 7).

[5]Formally, it is the combination $q\mathbf{B}$ that has pseudovector character due to the dependence on pseudovector $\mathbf{s}$ [see Eq. (37)]. So, in our case time-inversion symmetry is broken rather by the effective charge than by the effective field.

For definiteness I consider domains related by a rotation around the cubic axis through 90° (corresponding rotation matrix is $\Re_{12}$). Let us suppose that the AFM film is connected to two ferromagnetic electrodes that can produce a spin-polarized current (with the spin vector $\mathbf{s}_0$) in the in-plane geometry. The thickness of the AFM layer is smaller or comparable with the spin-coherence length (to exclude spin scattering processes); the thickness of the domain wall is much larger than the lattice constant (to validate the adiabatic approximation). Electric voltage applied to the system initiates an electron flow between the ferromagnetic electrodes with an average constant velocity $\mathbf{v}$ directed along the domain wall normal (denoted as the x axis). As the curvature of the flat domain wall is zero, the AFM texture affects only the spin evolution described by Eq. (31), which can be rewritten in the following form:

$$\frac{d\mathbf{s}}{dx} = \mathbf{\Omega}_x \times (\mathbf{s} - \sin 2\psi\, \hat{g}\mathbf{s}), \tag{41}$$

where the rotation vector $\mathbf{\Omega}_x$ has a fixed direction. It follows from Eq. (41) that after traveling through the domain wall vector, $\mathbf{s}$ will change by the value $\Delta\mathbf{s}$, which consists of two parts: rotation with the local AFM frame (due to the first term in parentheses) and geometric phase rotation (the second term) over a spheroid (30). In the case of strong exchange coupling ($\sin 2\psi \ll 1$), the first effect dominates. In this case

$$\Delta\mathbf{s} \approx \Re_{12}\mathbf{s}_0, \tag{42}$$

and the spin polarization can evolve by 90°, as shown in Fig. 7. If, then, the magnetization $\mathbf{M}_2$ of the second FM2 electrode is varied by an external magnetic field (as, e.g., in experiments [42]), magnetoresistance between the FM electrodes will also vary depending on $(\Delta\mathbf{s}\cdot\mathbf{M}_2)$.

Thus the AFM domain wall is a "spin-active" (in analogy with optically active) medium. Spin rotation, the quantum analog of the Faraday rotation in optics, results from the competition of two coherent spin states and could be observed by the electrical measurements.

B. Enveloping a soliton

Equations (31) and (34) predict nontrivial spin-induced orbital dynamics in a curved AFM texture. As an example, let us consider spin-polarized electrons traveling through a region with the inhomogeneous distribution of AFM vectors obtained in the following way. Suppose we start from the one-dimensional distribution of AFM vectors described by the Gibb's vector $\boldsymbol{\varphi}_1 = \tan(\theta_1(\xi)/2)\,\mathbf{e}_y$ [a "wire" with twisted AFM structure, Fig. 8(a)]. Next, the "wire" is bent to make a ring; this corresponds to a rotation with the Gibb's vector $\boldsymbol{\varphi}_2 = \tan[\theta_2(x,y)/2]\,\mathbf{e}_z$, where $\theta_2(x,y) = \tan^{-1} y/x$ [Fig. 8(b)]. The resulting rotation $\boldsymbol{\varphi} = \boldsymbol{\varphi}_2 \circ \boldsymbol{\varphi}_1$ is a composition of twisting and bending:

$$\boldsymbol{\varphi} = \boldsymbol{\varphi}_2 \circ \boldsymbol{\varphi}_1 = \tan\frac{\theta_1(\xi)}{2}\mathbf{e}_y + \tan\frac{\theta_2(x,y)}{2}\mathbf{e}_z - \tan\frac{\theta_1(\xi)}{2}\tan\frac{\theta_2(x,y)}{2}\mathbf{e}_x. \tag{43}$$

The effective coordinate of the first rotation, $\xi = y\cos\theta_2 - x\sin\theta_2$, bends with the "wire." Such a texture has a nonzero

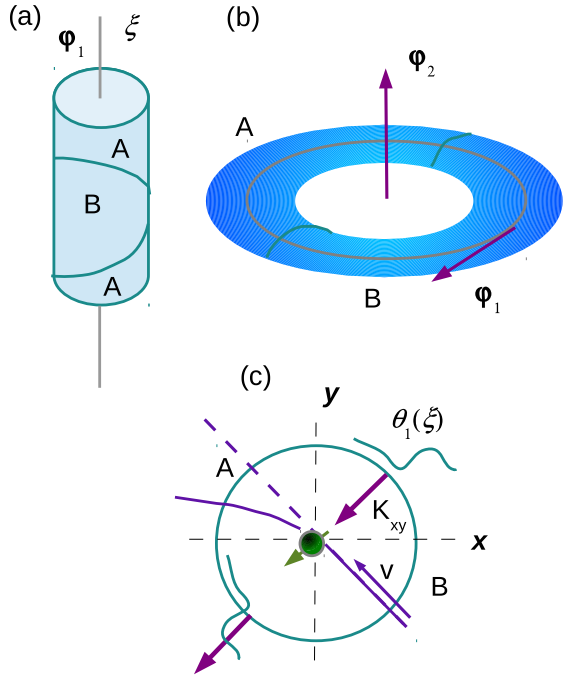

FIG. 8. (Color online) Electron traveling in the neighborhood of an AFM soliton: (a) "twisting" of an AFM structure (one-dimensional rotation with the Gibb's vector $\boldsymbol{\varphi}_1$); (b) "bending" of the twisted structure; and (c) spin-polarized electron moving with velocity $\mathbf{v}$ feels like a Lorentz force at the points of maximal curvature $\mathbf{K}_{xy}$ (arrows). A and B symbolize different domains.

curvature parallel to the radial component $\mathbf{e}_r$:

$$\mathbf{K}_{xy} \equiv \boldsymbol{\Omega}_x \times \boldsymbol{\Omega}_y = -\partial_\xi \theta_1(\xi) \sin 2\theta_2 \frac{\mathbf{e}_r}{r}, \tag{44}$$

where r is the radial coordinate.[6]

Let us further assume that the first, unbent distribution $\theta_1(\xi)$ corresponds to a kink or two "head-to-head" domain walls separating domains A and B. In this case $\partial_\xi \theta_1(\xi) \neq 0$ in the vicinity of the domain wall localization. For definiteness we assume that the domain walls are centered at $\theta_2 = \pi/4$ (domain wall between A and B) and $\theta_2 = 5\pi/4$ [domain wall between A and B, see Fig. 8(c)]. Obviously, $\partial_\xi \theta_1(\xi) \neq 0$ has opposite signs in these points. As a result, curvature $\mathbf{K}_{xy} \neq 0$ along the line $x = y$ and has the same direction at all points.

According to Eq. (37), AFM curvature produces fictitious out-of plane magnetic fields:

$$q B_z = \frac{1}{2r} \partial_\xi \theta_1(\xi) \sin 2\theta_2 \left[\mathbf{e_r} \cdot \mathbf{s} + \sin 2\psi \mathbf{e}_r \cdot \hat{g} \mathbf{s}\right]. \tag{45}$$

So, spin-polarized electrons with $\mathbf{s} \parallel \mathbf{K}_{xy}$ traveling with constant velocity $\mathbf{v} \perp \mathbf{K}_{xy}$ through the texture are exerted by the Lorentz force and deflect from the initial trajectory[7] [see Fig. 8(c)].

As the curvature direction is constant, all equally polarized electrons will deflect in the same way, thus demonstrating a topological spin Hall effect. So, such a texture can be probed with spin-polarized current. On the other hand, electrons with different spins are deflected in opposite directions, so the texture can also work as a spin separator. It should be stressed that the topological spin Hall effect can be modified by spin-orbit interaction, neglected in the present calculations.

V. CONCLUSIONS

In the present paper I consider the adiabatic dynamics of free electrons in AFM with triangular magnetic structure. I show that, in analogy with the collinear AFM [17], the dynamics of a real spin $\mathbf{s}$ is influenced by space-time variation of antiferromagnetically coupled vectors $\mathbf{S}_j(\mathbf{r},t)$. The main features of the electron behavior arising from accumulation of non-Abelian SU(2) Berry phase—precession of the electron spin around the dynamic AFM magnetization and spin-dependent orbital dynamics—are similar in both cases. The first effect is of pure geometric nature, as the homogeneous AFM has no uncompensated magnetization and produces no magnetic field. The second effect is related with processes of spin pumping and spin-transfer torque and is thus experimentally observable.

Similarity (up to the details) of free electron dynamics in the collinear and triangular AFMs gives the grounds to anticipate analogous effects in even more complicated AFM metals such as FeMn, which shows 3$\mathbf{q}$ structure described in terms of four magnetic sublattices.

The described toy model can be applied to antiperovskites Mn_3MN (M = Ni, Ag, Zn), which show a noncollinear 120° magnetic structure and semiconducting type of conductivity (see, e.g., Ref. [43]). Although in this paper we appeal mainly to the perovskites Mn_3XN, the results obtained could be applied to the metallic AFM $IrMn_3$ with the same triangular structure [44,45] which is widely used in spintronics due to its high Néel temperature.

The influence of the spin-related curvature on the orbital motion of free electrons is related with the topological features of the system and thus is quite a general property. It can be used for detection of inhomogeneous distribution of magnetic systems such as topological solitons and/or Skyrmions recently observed in AFMs [46]. Adiabatic spin transport is a possible tool for study of AFM two- and three-dimensional textures induced by mechanical tilting through the flexomagnetic effect typical for triangular AFM structures [26]. A system of triangular Ising spins realized with trapped ions [47] can also be also used as a playground for quantum simulation of non-Abelian SU(2) Berry-phase effects.

ACKNOWLEDGMENTS

I am grateful to Yu. Mokrousov, F. Freimut, and J. Sinova for fruitful discussions. I also acknowledge help from P. Buhl and A. Malyshenko.

[6]The proposed model distribution of the AFM order parameter has a peculiarity at $r \to 0$ which can be avoided by placing a defect or a hole in the center.

[7]The spin rotation which arises during the passage through the domain wall can reduce the deflection. However, due to the $1/r$ dependency of the Lorentz force, the effect can still be pronounced close to the center of the region.

APPENDIX A: HAMILTONIAN DIAGONALIZATION

Hamiltonian (6) mixes all six wave functions $|u_j\rangle|\tau\rangle, j = 1,2,3, \tau = \uparrow,\downarrow$. However, symmetry considerations make it possible to simplify the diagonalization procedure which we describe in this section.

First, we notice that if the quantization axis is taken in the local frame with the z'_j axis parallel to $\mathbf{S}_j$, then the sd-exchange term is diagonal in the spin space: $\mathbf{S}_j\hat{\boldsymbol{\sigma}}_{\tau\tau'} = S\hat{\sigma}_{jz'}$. As the vectors $\mathbf{S}_j$ (and correspondingly, local quantization axes) could be generated from the lab axis by rotations around the plane normal $\mathbf{n}$, it is convenient to introduce new creation/annihilation operators,

$$\begin{pmatrix}\hat{b}_{j\uparrow}\\ \hat{b}_{j\downarrow}\end{pmatrix} = \hat{U}_j^{\dagger}\begin{pmatrix}\hat{a}_{j\uparrow}\\ \hat{a}_{j\downarrow}\end{pmatrix}, \quad j = 1,2,3, \tag{A1}$$

where the unitary operators $\hat{U}_j = \cos\frac{\theta_j}{2}\hat{1} - i\sin\frac{\theta_j}{2}\mathbf{n}\hat{\boldsymbol{\sigma}}$ represent rotation through the angles $\theta_1 = 0$, $\theta_2 = 2\pi/3$, and $\theta_3 = 4\pi/3$.

For further simplification we take the permutation symmetry of the magnetic sublattices [24] into account and introduce the following combinations of operators $\hat{b}_{j\tau}$,

$$\begin{aligned}\hat{\xi}_{1\tau} &= \frac{1}{\sqrt{6}}(2\hat{b}_{1\tau} - \hat{b}_{2\tau} - \hat{b}_{3\tau}), \quad \hat{\xi}_{2\tau} = \frac{1}{\sqrt{2}}(\hat{b}_{2\tau} - \hat{b}_{3\tau}),\\ \hat{\xi}_{3\tau} &= \frac{1}{\sqrt{3}}(\hat{b}_{1\tau} + \hat{b}_{2\tau} + \hat{b}_{3\tau}),\end{aligned} \tag{A2}$$

that form irreducible representations of permutation group P_3 (isomorphic to C_3 rotation group which describes the exchange symmetry of the compound).

Operators $\{\hat{b}_{j\tau},\hat{b}^{\dagger}_{j\tau}\}$ and $\{\hat{\xi}_{j\tau},\hat{\xi}^{\dagger}_{j\tau}\}$ satisfy the same anticommutation relations as Fermi operators $\{\hat{a}_{j\tau},\hat{a}^{\dagger}_{j\tau}\}$.

It is worth mentioning that the operators $\{\hat{\xi}_{1\tau},\hat{\xi}_{2\tau}\}$ belong to the same irreducible representation as the AFM vectors $\{\mathbf{L}_1,\mathbf{L}_2\}$, and the operator $\{\hat{\xi}_{3\tau}\}$ has the same transformation properties as the magnetization vector $\mathbf{M}$ [see Eq. (2)].

As it was already mentioned, in the AFM ground state $\mathbf{M} = \mathbf{0}$, $\mathbf{L}_1\perp\mathbf{L}_2\perp\mathbf{n}$, $|\mathbf{L}_1| = |\mathbf{L}_2| = \sqrt{3/2}S$ [24]. We take the quantization axis for free spins parallel to $\mathbf{L}_1$.

Taking account of transformations (A1) and (A2), the Hamiltonian (6) takes a form

$$\begin{aligned}\hat{H}(\mathbf{r},t) = &-J_{sd}S\sum_j(\hat{\xi}^{\dagger}_{j\uparrow}\hat{\xi}_{j\uparrow} - \hat{\xi}^{\dagger}_{j\downarrow}\hat{\xi}_{j\downarrow})\\ &+\gamma(\mathbf{k})[2\hat{\xi}^{\dagger}_{3\tau}\hat{\xi}_{3\tau} - (\hat{\xi}^{\dagger}_{1\tau}\hat{\xi}_{1\tau} + \hat{\xi}^{\dagger}_{2\tau}\hat{\xi}_{2\tau})\\ &+3(\hat{\xi}^{\dagger}_{1\downarrow}\hat{\xi}_{2\uparrow} + \hat{\xi}^{\dagger}_{2\uparrow}\hat{\xi}_{1\downarrow} - \hat{\xi}^{\dagger}_{2\downarrow}\hat{\xi}_{1\uparrow} - \hat{\xi}^{\dagger}_{1\uparrow}\hat{\xi}_{2\downarrow})],\end{aligned} \tag{A3}$$

which now can be easily diagonalized.

APPENDIX B: BERRY CONNECTION, BERRY CURVATURE, AND DYNAMICS EQUATIONS

To simplify the calculation of the Berry connection (19) we note that (i) time and space dependence of the state vectors $|\Psi_{2a}(r_\mu)\rangle$, $|\Psi_{2b}(r_\mu)\rangle$ stems from the rotation of the spin quantization axis; (ii) rotation of the local frame (unit vectors $\mathbf{e}_k(r_\mu)$, $k = x,y,z$) can be equivalently represented in terms of the rotation matrix $\Re$ (3): $\mathbf{e}_k(r_\mu) \equiv \Re(\boldsymbol{\varphi})e^0_k$ or related unitary matrix $\hat{U}$ (14): $\mathbf{e}\hat{\boldsymbol{\sigma}} = \hat{U}\mathbf{e}^0\hat{\boldsymbol{\sigma}}\hat{U}^{\dagger}$, where $\mathbf{e}^0_k$ is taken at some reference point r^0_μ. The same matrix $\hat{U}$ defines transformation (15) of state the vectors $|\Psi_2(r_\mu)\rangle$. An analogous procedure was proposed in Ref. [48]. So, the Berry connection $\hat{\mathcal{A}}^r_\mu$ can be expressed as

$$\hat{\mathcal{A}}^r_\mu = i\begin{pmatrix}\langle\Psi^0_{2a}|\hat{\Lambda}_\mu\Psi^0_{2a}\rangle & \langle\Psi^0_{2a}|\hat{\Lambda}_\mu\Psi^0_{2b}\rangle\\ \langle\Psi^0_{2b}\mid\hat{\Lambda}_\mu\Psi^0_{2a}\rangle & \langle\Psi^0_{2b}|\hat{\Lambda}_\mu\Psi^0_{2b}\rangle\end{pmatrix}, \tag{B1}$$

where we introduced the matrix $\hat{\Lambda}_\mu \equiv \hat{U}^{\dagger}\partial^r_\mu\hat{U}$. Direct calculations show that

$$\hat{\Lambda}_\mu = -\frac{i}{2}\Re^{-1}(\boldsymbol{\varphi})\boldsymbol{\Omega}_\mu\hat{\boldsymbol{\sigma}} \tag{B2}$$

and

$$\begin{aligned}\hat{\mathcal{A}}^r_\mu = &\big(\tfrac{1}{2}\sin 2\psi\,\Re^{-1}(\boldsymbol{\varphi})\boldsymbol{\Omega}_\mu\\ &+\tfrac{1}{4}(1-\sin 2\psi)\mathbf{n}_0\times\Re^{-1}(\boldsymbol{\varphi})\Omega_\mu\times\mathbf{n}_0\big)\hat{\boldsymbol{\sigma}}.\end{aligned} \tag{B3}$$

From (B3) after some simple math one gets expression (21).

It is obvious from relations (B1) and (B2) that the singlet states with zero spin do not contribute to the Berry connection.

The spin vector $\mathbf{s}(t,\mathbf{r}) = \langle w|\,\hat{\boldsymbol{\sigma}}\,|w\rangle$ is calculated in a similar way with the help of matrix $\hat{\Sigma} \equiv \hat{U}^{\dagger}\hat{\boldsymbol{\sigma}}\hat{U} = \Re(\boldsymbol{\varphi})\boldsymbol{e}^0_k\hat{\sigma}_k$, the explicit relation being

$$\mathbf{s}(t,\mathbf{r}) = \Re(\boldsymbol{\varphi})\big[\sin 2\psi\,\mathbf{C} + \tfrac{1}{2}(1-\sin 2\psi)\,\mathbf{n}_0\times(\mathbf{C}\times\mathbf{n}_0)\big]. \tag{B4}$$

Using the relation $\mathbf{n} = \Re(\boldsymbol{\varphi})\mathbf{n}_0$ between the vectors in the local and reference frame one gets expression (29) from (B4).

Equation (B4) is easily inverted in order to express the isospin $\mathbf{C}$ through the real spin as follows:

$$\mathbf{C} = \frac{2}{1+\sin 2\psi}\Re^{-1}(\varphi)\left[\mathbf{s}(t,\mathbf{r}) + \frac{1-\sin 2\psi}{2\sin 2\psi}(\mathbf{ns})\,\mathbf{n}\right]. \tag{B5}$$

Substituting relation (B5) into the normalization condition $|\mathbf{C}|^2 = 1$ one gets Eq. (30) for spheroid.

The Berry curvatures (22) are calculated by differentiation of (B3) with account of two general relations:

$$\dot{\Re}(\boldsymbol{\varphi}) = \boldsymbol{\Omega}\times\Re(\boldsymbol{\varphi}) \quad \text{and} \quad \partial^r_\nu\boldsymbol{\Omega}_\mu - \partial^r_\mu\boldsymbol{\Omega}_\nu = \boldsymbol{\Omega}_\mu\times\boldsymbol{\Omega}_\nu. \tag{B6}$$

Dynamic equation (31) for the spin is obtained by differentiation of the expression (29) with the use of relations (B6), (16), and (B5).

The complete equation for acceleration has the following form:

$$\begin{aligned}\dot{k}_\mu = &-\partial^r_\mu\varepsilon_2 - \frac{1}{2}\dot{\mathbf{s}}\cdot\boldsymbol{\Omega}_\mu\\ &-\frac{1}{2}\dot{k}_\nu\partial^k_\nu\ln(1+\sin 2\psi)\left[\mathbf{s}\cdot\boldsymbol{\Omega}_\mu + \frac{1}{\sin 2\psi}(\mathbf{ns})(\mathbf{n}\Omega_\mu)\right].\end{aligned} \tag{B7}$$

[1] X. Tang, H.-W. Zhang, H. Sua, Y.-L. Jing, and Z.-Y. Zhong, J. Magn. Magn. Mater. **321**, 1851 (2009).

[2] T. Kampfrath, A. Sell, G. Klatt, A. Pashkin, S. Mahrlein, T. Dekorsy, M. Wolf, M. Fiebig, A. Leitenstorfer, and R. Huber, Nat. Photon **5**, 31 (2011).

[3] P. Haney, R. Duine, A. S. Nunez, and A. MacDonald, J. Magn. Magn. Mater. **320**, 1300 (2008).

[4] H. Gomonay and V. Loktev, J. Magn. Soc. Jpn. **32**, 535 (2008).

[5] E. V. Gomonay and V. M. Loktev, Low Temp. Phys. **34**, 198 (2008).

[6] R. Cheng, J. Xiao, Q. Niu, and A. Brataas, Phys. Rev. Lett. **113**, 057601 (2014).

[7] K. M. D. Hals, Y. Tserkovnyak, and A. Brataas, Phys. Rev. Lett. **106**, 107206 (2011).

[8] E. G. Tveten, A. Qaiumzadeh, O. A. Tretiakov, and A. Brataas, Phys. Rev. Lett. **110**, 127208 (2013).

[9] J. Železný, H. Gao, K. Výborný, J. Zemen, J. Mašek, A. Manchon, J. Wunderlich, J. Sinova, and T. Jungwirth, Phys. Rev. Lett. **113**, 157201 (2014).

[10] H. Chen, Q. Niu, and A. H. MacDonald, Phys. Rev. Lett. **112**, 017205 (2014).

[11] J. Kübler and C. Felser, EPL **108**, 67001 (2014).

[12] P. Bruno, V. K. Dugaev, and M. Taillefumier, Phys. Rev. Lett. **93**, 096806 (2004).

[13] N. Nagaosa, J. Sinova, S. Onoda, A. H. MacDonald, and N. P. Ong, Rev. Mod. Phys. **82**, 1539 (2010).

[14] H. Takatsu, S. Yonezawa, S. Fujimoto, and Y. Maeno, Phys. Rev. Lett. **105**, 137201 (2010).

[15] C. Sürgers, G. Fischer, P. Winkel, and H. v. Löhneysen, Nat. Commun. **5**, 3400 (2014).

[16] Y. Tserkovnyak and C. H. Wong, Phys. Rev. B **79**, 014402 (2009).

[17] R. Cheng and Q. Niu, Phys. Rev. B **86**, 245118 (2012).

[18] S. E. Barnes and S. Maekawa, Phys. Rev. Lett. **98**, 246601 (2007).

[19] F. Freimuth, R. Bamler, Y. Mokrousov, and A. Rosch, Phys. Rev. B **88**, 214409 (2013).

[20] E. Bertaut, D. Fruchart, J. Bouchaud, and R. Fruchart, Solid State Commun. **6**, 251 (1968).

[21] J. P. Jardin and J. Labbé, J. Phys. (France) **36**, 1317 (1975).

[22] Z. Ali, M. Shafiq, S. J. Asadabadi, H. R. Aliabad, I. Khan, and I. Ahmad, Comput. Mater. Sci. **81**, 141 (2014).

[23] K. Motizuki and H. Nagai, J. Phys. C **21**, 5251 (1988).

[24] E. V. Gomonaj and V. A. L'vov, Phase Transitions **38**, 15 (1992).

[25] E. V. Gomonaj and V. A. L'vov, Phase Transitions **40**, 225 (1992).

[26] P. Lukashev and R. F. Sabirianov, Phys. Rev. B **82**, 094417 (2010).

[27] E. Chi, W. Kim, and N. Hur, Solid State Commun. **120**, 307 (2001).

[28] K. Takenaka, A. Ozawa, T. Shibayama, N. Kaneko, T. Oe, and C. Urano, Appl. Phys. Lett. **98**, 022103 (2011).

[29] A. F. Andreev and V. I. Marchenko, Phys.-Usp. **23**, 21 (1980).

[30] H. V. Gomonay, R. V. Kunitsyn, and V. M. Loktev, Phys. Rev. B **85**, 134446 (2012).

[31] L. Chu, C. Wang, J. Yan, Y. Na, L. Ding, Y. Sun, and Y. Wen, Scr. Mater. **67**, 173 (2012).

[32] G. Sundaram and Q. Niu, Phys. Rev. B **59**, 14915 (1999).

[33] D. Xiao, M.-C. Chang, and Q. Niu, Rev. Mod. Phys. **82**, 1959 (2010).

[34] D. Culcer, Y. Yao, and Q. Niu, Phys. Rev. B **72**, 085110 (2005).

[35] Y. Tserkovnyak and M. Mecklenburg, Phys. Rev. B **77**, 134407 (2008).

[36] N. Nagaosa and Y. Tokura, Nat. Nano **8**, 899 (2013).

[37] G. E. Volovik, J. Phys. C **20**, L83 (1987).

[38] A. M. Kosevich, B. A. Ivanov, and A. S. Kovalev, *Nonlinear Magnetization Waves, Dynamical and Topological Solitons* (Naukova Dumka, Kiev, 1983), p. 189 (in Russian).

[39] R. Rajaraman, *Solitons and Instantons: An Introduction to Solitons and Instantons in Quantum Field Theory* (North-Holland, Amsterdam, 1987).

[40] Y. B. Bazaliy, B. A. Jones, and S.-C. Zhang, Phys. Rev. B **57**, R3213 (1998).

[41] R. Shindou and N. Nagaosa, Phys. Rev. Lett. **87**, 116801 (2001).

[42] X. Martí, B. G. Park, J. Wunderlich, H. Reichlová, Y. Kurosaki, M. Yamada, H. Yamamoto, A. Nishide, J. Hayakawa, H. Takahashi, and T. Jungwirth, Phys. Rev. Lett. **108**, 017201 (2012).

[43] J. Lin, B. Wang, P. Tong, S. Lin, W. Lu, X. Zhu, Z. Yang, W. Song, J. Dai, and Y. Sun, Scr. Mater. **65**, 452 (2011).

[44] L. Szunyogh, B. Lazarovits, L. Udvardi, J. Jackson, and U. Nowak, Phys. Rev. B **79**, 020403(R) (2009).

[45] A. Kohn, A. Kovács, R. Fan, G. J. McIntyre, R. C. C. Ward, and J. P. Goff, Sci. Rep. **3**, 2412 (2013).

[46] I. Raičević, D. Popović, C. Panagopoulos, L. Benfatto, M. B. Silva Neto, E. S. Choi, and T. Sasagawa, Phys. Rev. Lett. **106**, 227206 (2011).

[47] K. Kim, M.-S. Chang, S. Korenblit, R. Islam, E. E. Edwards, G.-D. Freericks, J. K. Lin, L.-M. Duan, and C. Monroe, Nature (London) **465**, 590 (2010).

[48] G. Tatara and H. Fukuyama, Phys. Rev. Lett. **78**, 3773 (1997).